Electronic Supplementary Information (ESI)

Achieving Highly Efficient, Mechanically Robust and Thermally Stable Organic Solar Cells through Optimizing Branching Positions and Side Chain Length of Small Molecule Acceptors

Di Zhang,[‡a] Junfeng Liu,[‡a] Xiang Gao,[b] Zhi Wang,[a] Jiayi He,[a] Zhenye Wang,[a] Lvpeng Yang,[a] Yerun Gao,[a] Ming Shao*[a]

1. Materials and Methods.

Synthesis.

General information: All reagents and solvents, unless otherwise specified, were obtained from Aladdin, and Energy Chemical and were used as received.

The core unit S1a (3,9-diundecyl-12,13-dihydro-[1,2,5]thiadiazolo[3,4-e]thieno[2",3":4',5']thieno[2',3':4,5]pyrrolo[3,2-g]thieno[2',3':4,5]thieno[3,2-b]indole) were prepared according to the reported literature[1]. 2-(5,6-difluoro-3-oxo-2,3-dihydro-1H-inden-1-ylidene)malononitrile was purchased from Derthon OPV Co Ltd. All manipulations involving air-sensitive reagents were performed under an atmosphere of dry nitrogen.

Synthesis of compounds S3a, S3b and S3c: A mixture of compound S1a (3.74 g, 5 mmol), compound S2a, S2b and S2c (18 mmol), potassium carbonate (11 g, 80 mmol), potassium iodide (0.95 g, 5.75 mmol) and *N,N*-dimethylformamide (DMF, 80 mL) were added into a three-necked round bottom flask, and purged with nitrogen for 10 min. Next, the mixture was heated to 100 °C for 24 h. After removing the solvent, the residue was extracted with ethyl acetate and water. The organic layers were combined and dried over Na_2SO_4, filtered and purified with column chromatography on silica gel using dichloromethane/petroleum ether as the eluent to obtain **compound S3a, S3b and S3c** as red solids, respectively.

Synthesis of compounds S4a, S4b and S4c: A mixture of **compounds S3a, S3b or S3c** (2 mmol), DMF (5 ml) and phosphorus oxychloride ($POCl_3$, 2 ml) were dissolved in the 1,2-dichloroethane (DCE, 10 mL) under nitrogen at 0 °C and stirred at the same temperature for 2 h. The mixture was heated at 90 °C and reacted overnight. After the reaction, the mixture was cooled to room temperature, poured into ice water and extracted with dichloromethane. Then, the combined organic layer was washed with brine, dried over Na_2SO_4, and evaporated under reduced pressure. The crude product was purified with column chromatography on silica gel using dichloromethane/petroleum ether as the eluent to give **compounds S4a, S4b and S4c** as red solids, respectively.

Synthesis of BTP-C3, BTP-EH and BTP-HD: A mixture of **compounds S4a, S4b or**

S4c (0.3 mmol), IC-2F (0.42 g, 1.8 mmol), pyridine (PYR, 1.5 mL) and chloroform (CF, 60 mL) were dissolved in a round bottom flask under nitrogen. The mixture was stirred at 70 °C overnight. After the reaction, the mixture was cooled to the room temperature and removing the solvent. Then the residue was poured into methanol and filtered. The crude was purified with column chromatography on silica gel using dichloromethane/petroleum ether as the eluent to give **BTP-C3, BTP-EH and BTP-HD** as dark blue solids, respectively. **BTP-C3:** ^{1}H NMR (600 MHz, $CDCl_3$) δ 8.46 (s, 2H), 8.39-8.23 (m, 2H), 7.50 (t, *J* = 7.1 Hz, 2H), 4.62 (t, *J* = 7.4 Hz, 4H), 2.91 (t, *J* = 7.4 Hz, 4H), 2.12-1.96 (m, 4H), 1.77-1.67 (m, 4H), 1.51-1.40 (m, 8H), 1.35-1.12 (m, 46H), 0.89-0.85 (m, 12H), 0.77 (s, 6H). **BTP-EH:** ^{1}H NMR (600 MHz, $CDCl_3$) δ 8.54 (s, 2H), 8.43-8.28 (m, 2H), 7.59-7.47 (m, 2H), 4.62 (t, *J* = 7.4 Hz, 4H), 2.92-2.89 (m, 4H), 2.11-2.01 (m, 4H), 1.72-1.67(m, 4H),, 1.53-1.39 (m, 12H), 1.37-1.12 (m, 46H), 0.99-0.72 (m, 18H). **BTP-HD:** ^{1}H NMR (600 MHz, $CDCl_3$) δ 8.70 (s, 2H), 8.54-8.28 (m, 2H), 7.59 (t, *J* = 7.3 Hz, 2H), 4.69 (t, *J* = 7.0 Hz, 4H), 2.98 (t, *J* = 7.1 Hz, 4H), 2.01 (m, 4H), 1.76-1.73 (m, 4H), 1.52-1.42 (m, 4H), 1.41-0.99 (m, 86H), 0.87 (t, *J* = 6.9 Hz, 6H), 0.80 (m, 12H).

Device fabrication.

Materials: Octadecyltrichlorosilane (OTS, 95%, 5-10% branched isomers), chitosan (< 200 mPa.s) and DMF were purchased from Macklin Co., Ltd. Hexane and acetic acid were obtained from Shanghai Reagent Company (Shanghai, China). Silver nanowire (AgNW, diameter of 30±3 nm and length of 25±5 μm) dispersion in IPA with the concentration of 10 mg/ml was purchased from Coldstones Tech Co., Ltd. Thermoplastic urethane (TPU, 1185A) was obtained from BASF. Clevios PH1000 and PVP Al 4083 were provided by Heraeus Clevios. Polyethylene oxide (PEO, Mv ~ 600,000) was obtained from Aladdin (China). A fluorosurfactant Capstone FS-31 was purchased from Dupont. D18 was obtained from Solarmer Materials Inc. The active layer material was used without further purification. PNDIT-F3N was purchased from eFlexPV Technology (Shenzhen) Co., Ltd. Indium (In, 99.99% purity) and gallium (Ga, 99.99% purity) were obtained from ZNXC Co., Ltd.

Preparation of electrode solutions: OTS was dissolved into hexane to obtain a solution with the concentration of 0.1% (volume fraction). Chitosan was dissolved in deionized water to the concentration of 0.2%, a few drops of acetic acid was added to facilitate its dissolution. TPU 1185A particles were dissolved in DMF to a concentration of 250 mg/ml. PEO was dissolved in DMF to achieve the concentration of 20 mg/ml. The PEO/PH1000 was obtained by mixing 30% (volume fraction) PEO solution in PH1000, the surfactant FS-31 was also added with the concentration of 0.5% to facilitate the PH1000 film deposition.

Rigid OSC fabrication: The rigid devices were fabricated in the architecture of ITO/PEDOT:PSS/ Active layer/ PNDIT-F3N /Ag on ITO glass substrates. And the thermal rigid devices were fabricated in the architecture of ITO/ZnO/ Active layer/ MoO_3 /Ag on ITO glass substrates. Glass/ITO was treated with plasma to enhance the surface energy. The PEDOT:PSS layer was spin coated to serve as hole transport layer at the spin speed of 3000 rpm for 1 min, and followed by 110 °C 10 min annealing process. Then, the samples were transferred into the N_2-filled glove box. The active layers (~110 nm) were also fabricated by spin coating at 1500 rpm for 60s from a CF solution (11 mg/mL in total solid content) with the donor/acceptor ratio at 1:1.6 in weight. It was then annealed at 100℃ for 10 minutes. After fabricating the active layer film, dissolved into methanol with the concentration of 1 mg/ml was spin coated onto the active layer at 3000 rpm for 1 min to serve as electron transport layer. Finally, 80 nm Ag cathode were evaporated on the device through shadow mask in a vacuum evaporator.

Intrinsically stretchable OSC (*is*-OSC) fabrication: For the *is*-OSCs fabrication technique,[3] the TPU/AgNW/PH1000 transparent electrode was patterned by laser ablation, PEDOT:PSS 4083 was spin coated with the spin speed of 2000 rpm for 1 min, followed by 110 °C and 10 min annealing process. The samples were transferred into the glove box, the active layer solution was subsequently spin coated onto the PEDOT:PSS 4083 hole transport layer, the same as those fabricated in “Rigid OSCs fabrication” section. After completion of active layer film deposition, PNDIT-F3N was

spin coated onto the active layer at the speed of 3000 rpm for 50 s. For the cathode fabrication, the EGaIn was spray coated onto the ETL through a shadow mask.

Characterization of compounds and films.

NMR measurements: ^{1}H spectra were recorded on a Bruker Ascend-600 MHz NMR spectrometer at room temperature.

Cyclic voltammograms (CV): CV measurements were recorded on a CHI 660E electrochemical workstation by using glassy carbon discs as the working electrode, Pt wire as the counter electrode, Ag/AgCl electrode as the reference electrode with a scanning rate of 100 mV/s in a 0.1 M tetrabutylammonium hexafluorophosphate (Bu_4NPF_6) solution, and the potential of Ag/Ag^+ reference electrode was internally calibrated by using ferrocene/ferroncenium (Fc/Fc^+) as the redox couple.

Current density-voltage (J-V) measurements: *J-V* curves were obtained using a source meter (2400, Keithley Instruments) under illumination of an AM 1.5G solar simulator (Enli Technology Co., Ltd.) with an intensity of 100 mW/cm^2 in glove box. The light intensity was carefully calibrated with a standard silicon reference (Enli Technology Co., Ltd.) which was certified in National Renewable Energy Laboratory (NREL). During the measurement, a shadow mask (aperture area: 0.045 cm^2) was used to define the photoactive area of OSCs, and the devices are scanned from -0.1 V to 1 V with a scan step of 0.025 V and the dwell times of 10 ms.

To assess the thermal stability of the OSCs, we tested the device in the N_2-filled glove box and relative humidity $< 1\%$. The device was annealed at 85 °C. Subsequently, the photovoltaic performance of the device was e obtained under illumination of an AM 1.5G solar simulator with an intensity of 100 mW/cm^2 and varied with the duration of the annealing process.

To measure the performance of *is*-OSCs under different strains, we set up a homemade tensile test system based on the precise displacement platform (OMSC40100, RED STAR YANG TEHCHNOLOGY). The fabricated *is*-OSCs were placed on tensile test system and illuminated by a calibrated solar simulator (SS-3A-F5). Then, different strains were applied to devices at a stretching rate of 0.5 mm/s. The corresponding *J-V* curves were recorded to determine the power conversion efficiency

(PCE). The strain was measured based on the distance between the grips of the tensile test system.

Morphological characterization techniques: All of the Grazing Incidence wide-angle X-ray diffraction (GIWAXS) measurements were carried out at BL14B1 beamline, Shanghai Synchrotron Radiation Facility (SSRF). Atomic force microscope (AFM) images were taken from Shimadzu equipment (SPM 9700) in tapping mode. Optical images were taken by an optical microscope (Sunny Optical Technology Co., LTD.). Film thicknesses were measured by DEKTAK XT profilometer.

Recombination and dissociation measurements: The short-circuit current density (J_{sc}) versus incident light intensity (P_{light}) follows a power law equation: $J_{sc} \propto P_{light}^{\alpha}$, the deviation of α from 1 reflects the degree of bimolecular recombination. The relationship of open circuit voltage (V_{oc}) against P_{light}, as $V_{oc} \propto SkT/q \ln(P_{light})$, the S value indicates the degree of monomolecular recombination. The exciton dissociation probabilities (P_{diss}) were calculated by measuring the photocurrent density ($J_{ph} = J_L - J_D$, where J_L and J_D are the current density under light illumination and in the dark, respectively) versus effective voltage ($V_{eff} = V_0 - V_a$, where V_0 is the compensation voltage when J_{ph} is zero and V_a is the applied voltage).

Space-charge limited current (SCLC) measurements: The mobility of films can be calculated from the Mott-Gurney equation in the SCLC regime.

$$J = \frac{9\varepsilon_0\varepsilon_r\mu V^2}{8d^3}$$

where J is the current density, ε_0 is the dielectric constant of free space with the value of 8.85×10^{-12} F/m, ε_r is the relative dielectric constant which is taken to be 3 for calculation, μ is the charge mobility, $V = V_{appl} - V_{bi}$, where V_{appl} is the applied voltage, V_{bi} is the work function difference between two electrodes, and d is the thickness of film.

Energy loss determination: We recalculated the E_g of OSCs using the derivative dEQE/dE method. Based on Shockley-Queisser (SQ) limit, the total energy loss (E_{loss}) of the devices was separated into three parts as shown in the equation below:

$$
\begin{aligned}
E_{loss} = \; & E_g \; - \; qV_{oc} \\
& = (E_g - qV_{OC}^{SQ}) + (qV_{OC}^{SQ} \\
& - qV_{OC}^{rad}) + (qV_{OC}^{rad} - qV_{oc}) \\
& = \Delta E_1 + \Delta E_2 + \Delta E_3
\end{aligned}
$$

ΔE_1 is the radiative energy loss above the bandgap. ΔE_2 is the radiative recombination loss from the absorption below the bandgap. ΔE_3 arise from the non-radiative recombination processes.

The ΔE_1, ΔE_2 and ΔE_3 are summarized in **Table S2**.

Film-on-water (FOW) tensile test: To measure the tensile stress-strain curves of active layer film, PEDOT:PSS (Al 4083) was first spin coated onto a cleaned glass substrate to act as a sacrificial layer and annealed at 110 °C for 10 min. The active layer was subsequently spin coated on PEDOT:PSS layer as reported in the "Rigid OSC fabrication" section. A dog-bone specimen was obtained with the laser patterning technique. To float the specimen on the water surface, the PEDOT:PSS layer was dissolved in water and active layer film was delaminated from the glass substrate and subsequently the film was floated on the water surface. To hold the specimen for measuring, the active layer was gripped between PDMS-coated grips via van der Waals adhesion. The tensile test was performed by applying tensile strain using a linear displacement stage (EPSC-60-50, OMTOOLS) at a speed of 2.0×10^{-5} m/s until fracture occurred at the specimen. A load cell (LVS-50GA, Kyowa) was used to measure the strain during the tensile test process.

Glass transition temperature (T_g) measurements: The active layer films were prepared on the clean glass substrate, and the UV-vis spectra was recorded with UV-vis-NIR spectrophotometer (UV-3600, Shimadzu). The films were heated for 5 min in the nitrogen-atmosphere glove box in the increments of temperature, and then cooled to room temperature, after which the films were transferred out of the glove box to conduct the UV-vis measurement. After obtaining the UV spectra of films under different annealing temperatures, the deviation metric (DM_T) was calculated from the equation below:

$$DM_T \equiv \sum_{\lambda_{min}}^{\lambda_{max}} \left[I_{RT}(\lambda) - I_T(\lambda)\right]^2$$

Where $I_T(\lambda)$ and $I_{RT}(\lambda)$ are the normalized absorption intensities of the film after annealed under the temperature T and as-cast (room temperature), respectively. λ is the wavelength, λ_{min} and λ_{max} are the lower and upper bounds of the optical sweep. The T_g can be calculated when the DM_T experienced a sharp increase along with the increasing of annealing temperature.

2. Supplementary Figures.

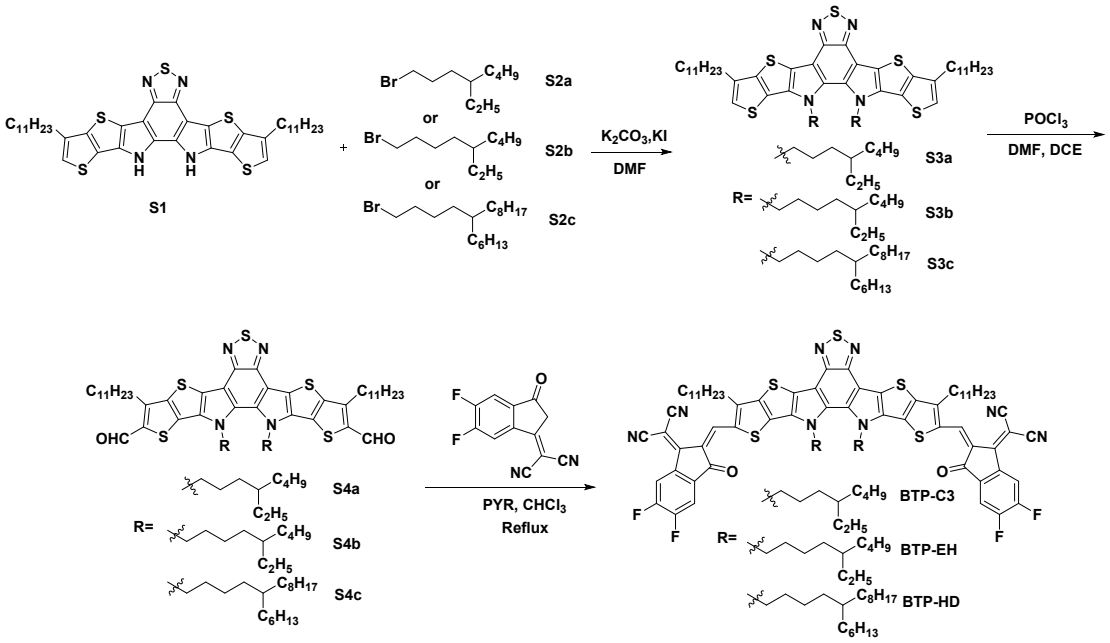

Scheme S1 Synthetic route of compounds BTP-C3, BTP-EH and BTP-HD.

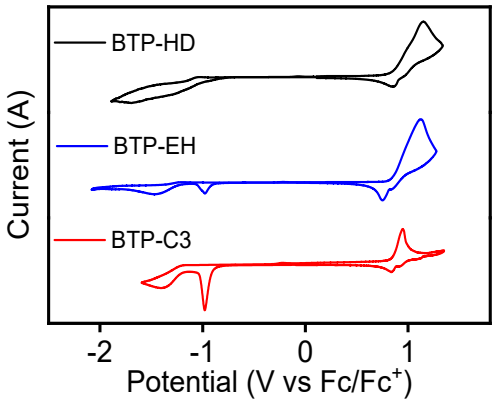

Fig. S1 Cyclic voltammograms of the indicated SMAs.

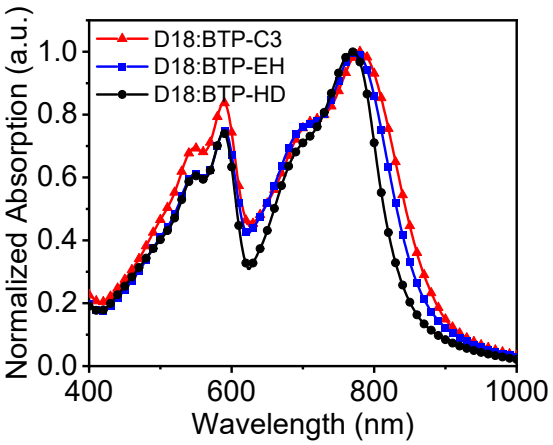

Fig. S2 UV-vis absorption spectra of blend films.

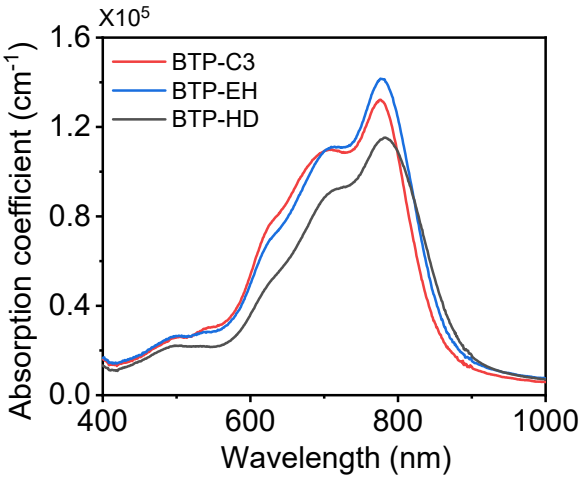

Fig. S3 The absorption coefficient of BTP-C3, BTP-EH and BTP-HD in the film.

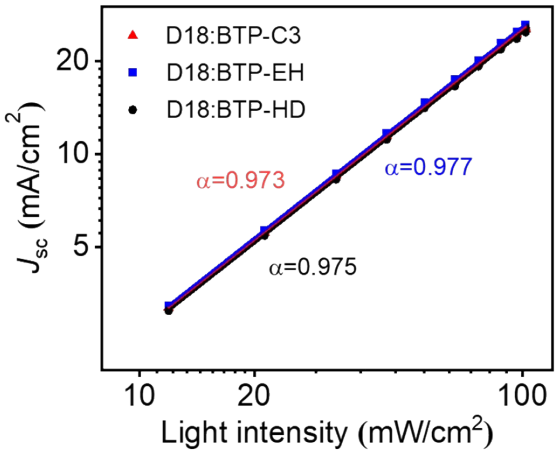

Fig. S4 Short circuit current versus light intensity of these indicated OSCs.

.

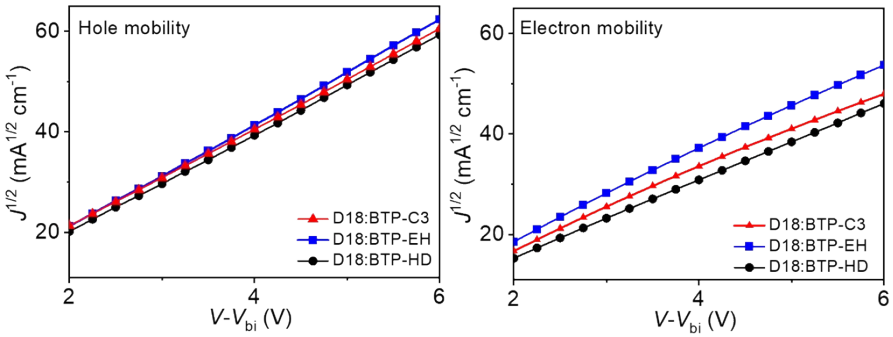

Fig. S5 The hole and electron mobilities of blend films.

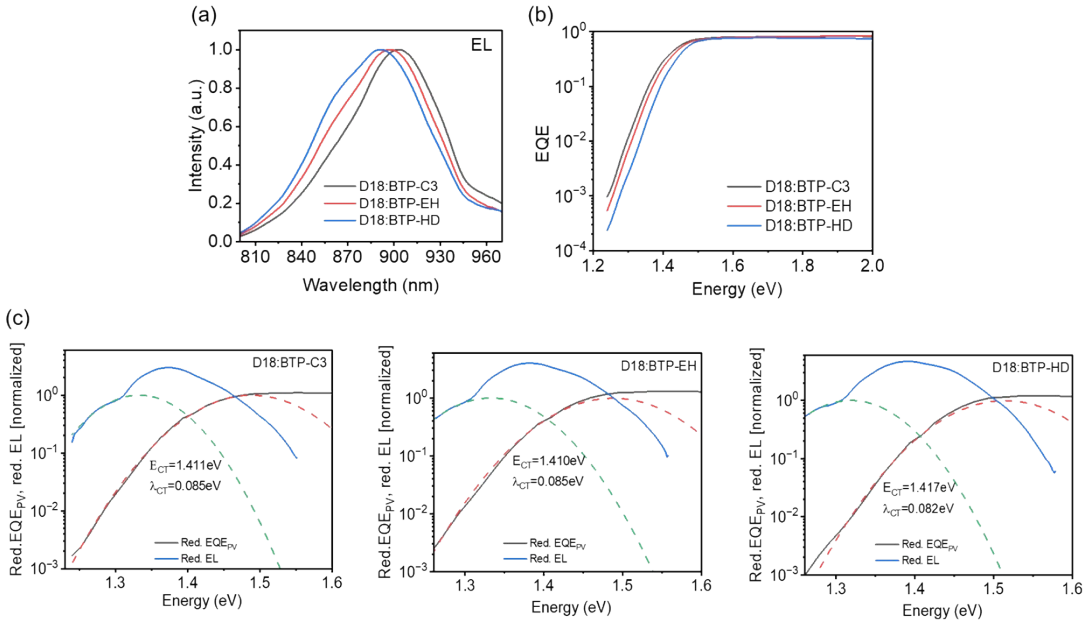

Fig. S6 (a) Normalized EL spectra of the fabricated devices. (b) EQE spectra. (c) Sensitive EQE_{pv} and electroluminescence (EL) spectra of the fabricated OSCs.

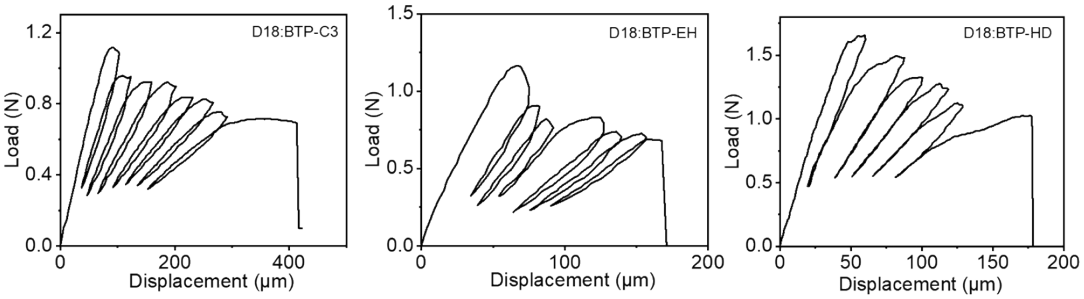

Fig. S7 Displacement *vs.* load profiles of blend films measured by DCB test.

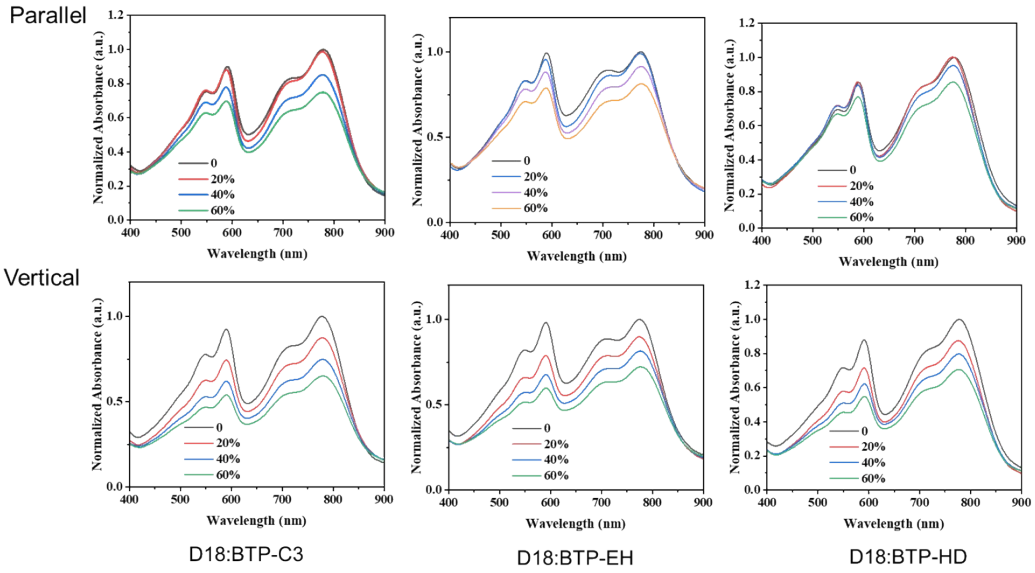

Fig. S8 UV-vis absorption spectra of stretched blend films under a polarizer in the direction parallel and perpendicular to the strain.

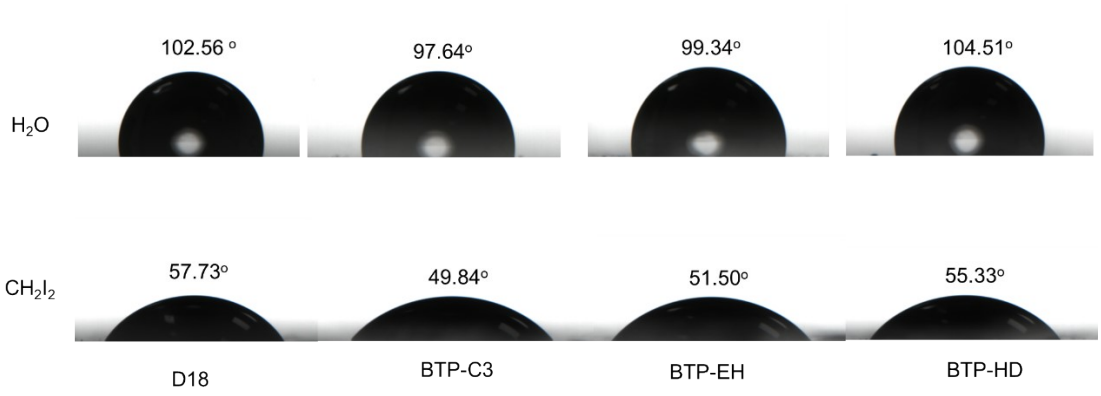

Fig. S9 Contact angle of water and diiodomethane on D18, BTP-C3, BTP-EH and BTP-HD.

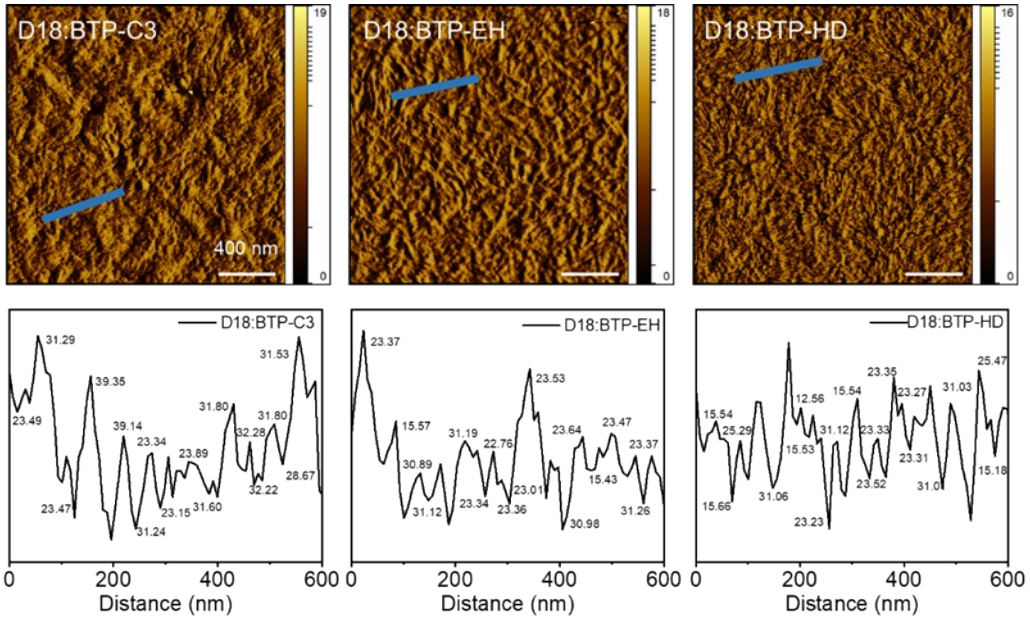

Fig. S10 The AFM phage image and line profile of phase images of the D18:BTP-C3, D18:BTP-EH and D18:BTP-HD blend films (scale bar: 400 nm).

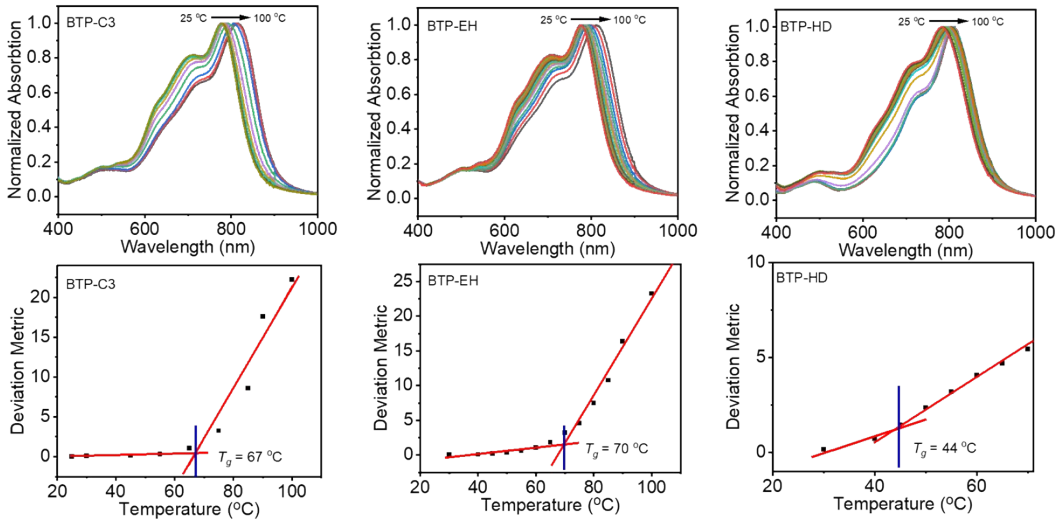

Fig. S11 UV-vis absorption of neat SMAs films with different aging temperatures and T_g of BTP-C3, BTP-EH and BTP-HD, respectively.

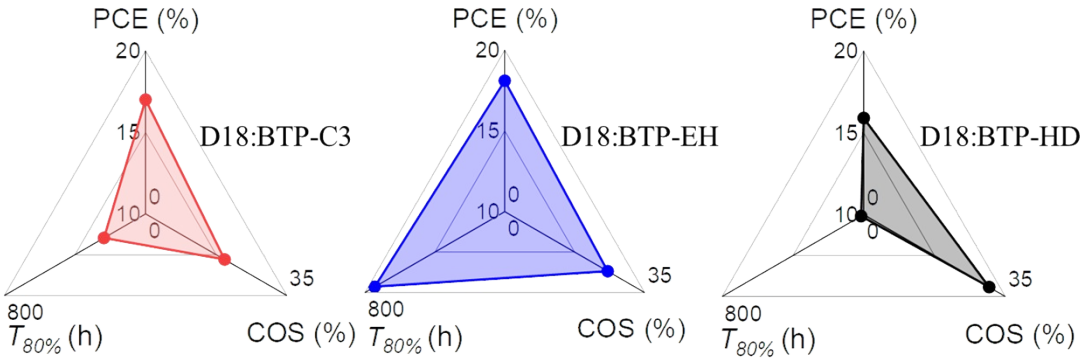

Fig. S12 Comparison of the photovoltaic, mechanical and thermal characteristics of D18:BTP-C3, D18:BTP-EH and D18:BTP-HD blend films.

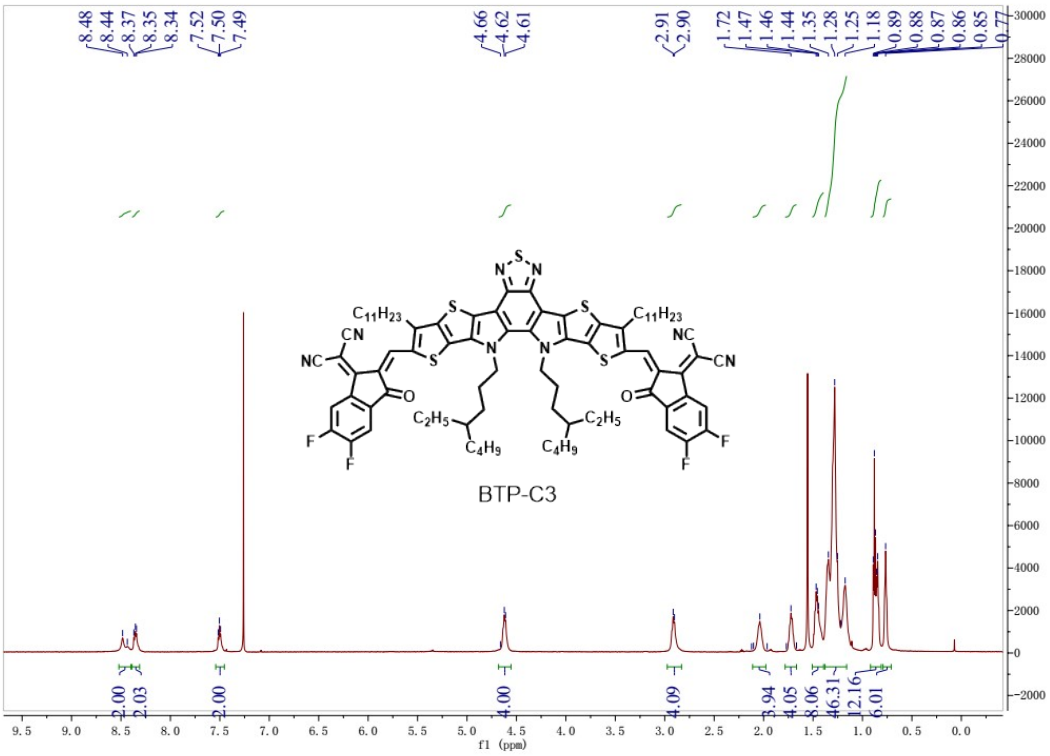

Fig. S13 ^{1}H NMR spectra of BTP-C3.

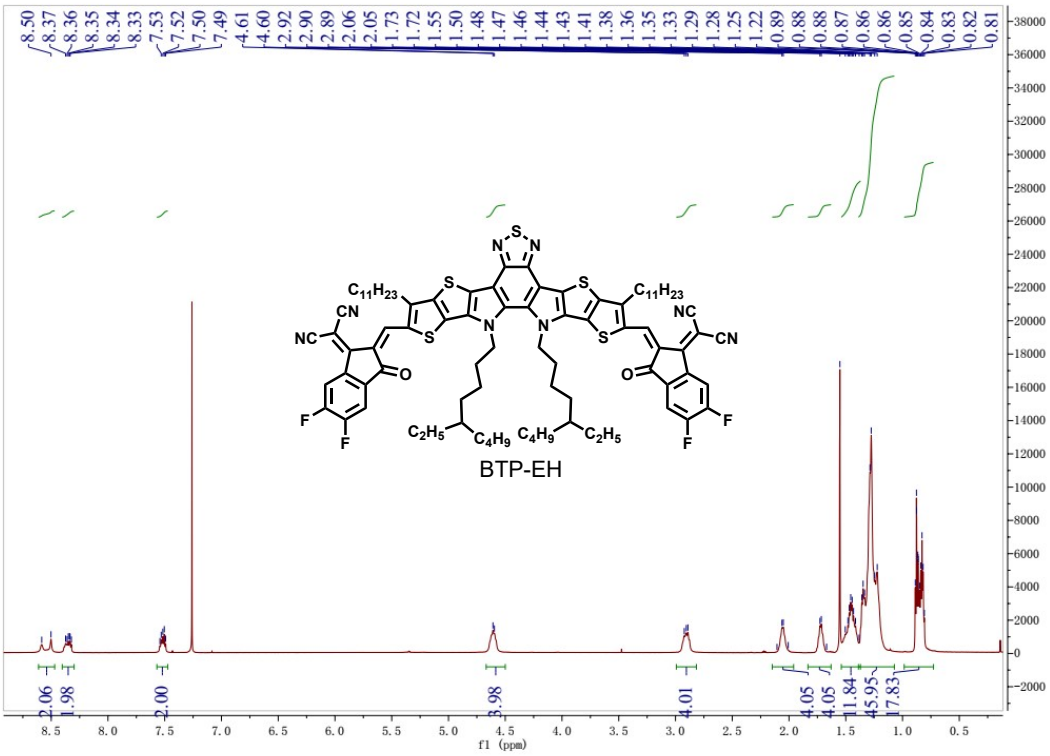

Fig. S14 ^{1}H NMR spectra of BTP-EH.

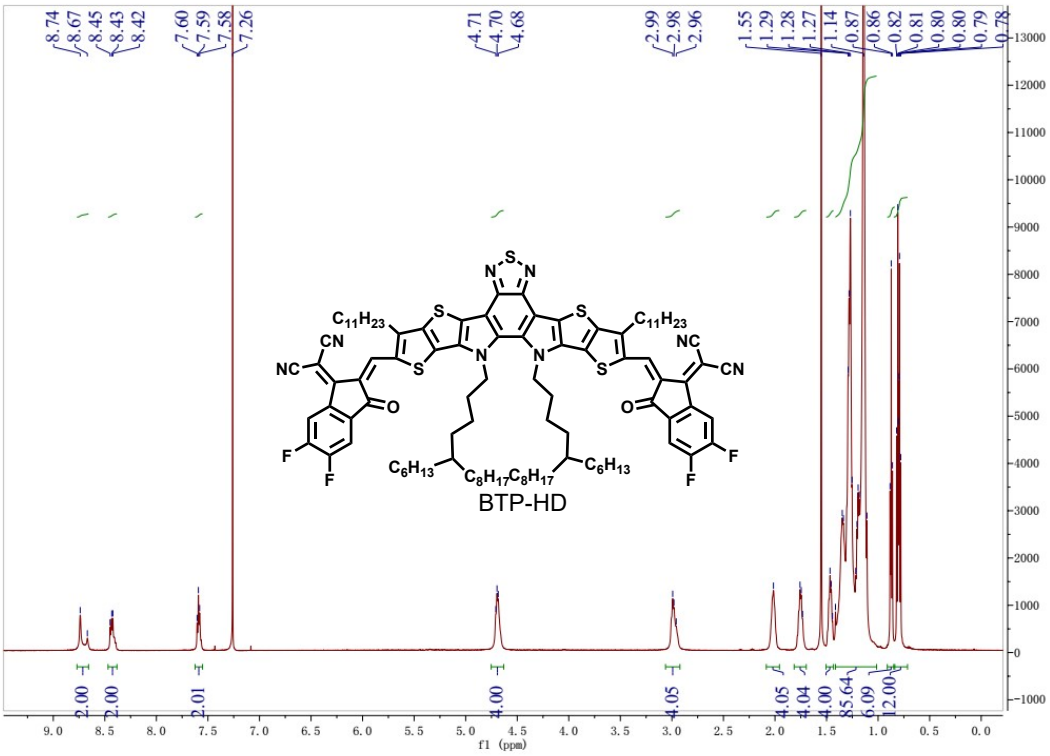

Fig. S15 ^{1}H NMR spectra of BTP-HD.

3. Supplementary Tables.

Table S1 The hole and electron mobilities of blend films.

Blend films	μ_h ($cm^2 V^{-1} s^{-1}$)	μ_e ($cm^2 V^{-1} s^{-1}$)	μ_h/μ_e
D18:BTP-C3	4.56×10^{-4}	3.23×10^{-4}	1.41
D18:BTP-EH	4.77×10^{-4}	3.97×10^{-4}	1.20
D18:BTP-HD	4.26×10^{-4}	2.69×10^{-4}	1.58

Table S2 The detailed energy loss parameters of the fabricated OSCs.

Blend films	E_g **(ev)**	$q^{V_{OC}}$ **(ev)**	$q^{V_{oc}^{SQ}}$ **(ev)**	$q^{V_{oc}^{rad}}$ **(ev)**	ΔE_1 **(ev)**	ΔE_2 **(ev)**	$\mathbf{EQE_{EL}}$ $*10^{-3}$ **(%)**	ΔE_3 **(ev)**
D18:BTP-C3	1.405	0.872	1.173	1.121	0.232	0.052	5.94	0.252
D18:BTP-EH	1.415	0.890	1.180	1.123	0.235	0.057	17.5	0.224
D18:BTP-HD	1.457	0.907	1.230	1.176	0.227	0.054	2.18	0.278

Table S3 PCE (Rigid-OSCs and *is*-OSCs) and crack-onset strain of active layer films reported in this work and other literatures.

Year	Blend films	$PCE_{Rigid\text{-}OSCs}$ (%)	$PCE_{is\text{-}OSCs}$ (%)	COS (%)	Reference
2020	PM6/Y6	15.4	-	5.75	[2]
2021	PM6:Y7:10%N2200	15.19	-	5.58	[3]
2021	PM6-C5:Y7	16.2	-	12.09	[4]
2021	PM6-C10:Y7	16.6	-	9.16	[4]
2021	PM6:N3	15.6	-	7.1	[5]
2021	PM6:N3:20%PCBM	16.7	-	9.3	[5]
2021	PM6:BTP-4Cl	15.3	-	10	[6]
2021	PM6:N3:SEBS (0%)	15.42	-	6.9	[7]
2021	PM6:N3:SEBS (2%)	15.98	-	8.1	[7]
2021	PM6:N3:SEBS (5%)	15.57	-	9.5	[7]
2021	PBDB-T/PYT (bilayer)	15.17	-	10.5	[8]
2022	PM6:PY-IT	15.56	-	9.5	[9]
2022	PM6:J71:PY-IT	16.52	-	8.9	[9]
2022	PBDB-TF:PY-IT	15.8	-	5.3	[10]
2022	PQM-Cl:PY-IT	18.0	-	6.5	[10]
2022	PBDB-T:PYFS-Reg	16.09	10.64	22.4	[11]
2022	PhAm5:Y7	17.45	12.73	13.8	[12]
2022	PM6:PY2Se-Cl-o	16.17		11.7	[13]
2022	PM6:PY2Se-Cl-ran	16.23		17.5	[13]
2022	PM6-OEG5:BTP-eC9	17.7	12.05	10.5	[14]
2022	PM6:BTP-eC9:PY-IT	16.52	15.3	8.9	[15]
2023	PETTCVT-H:L8-BO	15.32	10.1	7.1	[16]
2023	PM6-B10:Y6-BO	17.23	-	11.4	[17]
2023	PBQx-TF:PYIT (1:1)	15.6	-	16.5	[18]
2023	PBQx-TF:P1:PYIT (0.75:0.25:1)	16.4	-	19.5	[18]
2023	PBQx-TF:P2:PYIT (0.75:0.25:1)	17.1	-	20.4	[18]
2023	PM7-Thy10: L8-BO	17.05	13.69	13.7	[19]
2023	PM6-*b*-$PDMS_{19k}$:L8-BO	17.67	11.3	18.14	[20]
2023	PM6:BTP-eC9	12.83	10.9	2.99	[21]
2023	PM6:PTQ10:N3	16.90	-	9.50	[22]
2023	PM6:PM-OD:PY-IT	15.10	-	11.70	[23]
2023	PM6:L8-BO	19.06	15.54	5.67	[24]
2023	PM6:L8-BO:BTP-eC9	19.26	16.23	5.5	[24]
2023	PM6:2BOHD-TC4T	16.50		10	[25]
2024	D18:Y6:SEBS	16.54	-	26.38	[26]
2024	D180.8-S-	19.03	14.3	17.2	[27]

2024	PEHDT0.2:L8-BO PM6:Y6-BO:N2200-ThyDap	16.36	-	4.81	[28]
2024	PM6:L8-BO:SBS-COOH	19.04	-	21.48	[29]
2024	PM6:PM6-HD:BTP-eC9	14.15	12.0	7.12	[30]
2024	**D18:BTP-C3**	**17.0**	**14.9**	**19.6**	**This work**
2024	**D18:BTP-EH**	**18.1**	**15.6**	**25.8**	**This work**
2024	**D18:BTP-HD**	**15.9**	**13.6**	**31.0**	**This work**

Table S4 GIWAXS parameters of blend films.

Blend films	IP or OOP	Peak position ($Å^{-1}$)	d-spacing (Å)	FWHM ($Å^{-1}$)	CCL (Å)
D18:BTP-C3	IP	0.32	19.63	-	-
	OOP	1.76	3.57	0.181	31.24
D18:BTP-EH	IP	0.30	20.94	-	-
	OOP	1.76	3.57	0.166	34.06
D18:BTP-HD	IP	0.28	22.44	-	-
	OOP	1.73	3.63	0.201	28.13

Table S5 Contact angle of water and diiodomethane and surface energy of D18, BTP-C3, BTP-EH and BTP-HD.

Films	**θ° (water)**	**θ° (Diiodomethane)**	**Surface Energy γ (mN m^{-1})**	**χ**
D18	102.56	57.73	29.64	-
BTP-C3	97.64	49.84	34.18	0.16
BTP-EH	99.34	51.50	33.40	0.11
BTP-HD	104.51	55.33	31.83	0.04

Table S6 Photovoltaic parameters of *is*-OSCs.

Blend films	V_{OC} **(V)**	J_{SC} **(mA/cm^2)**	**FF (%)**	**PCE (%)**
D18:BTP-C3	0.853	23.1	75.4	14.4±0.33 (14.9)
D18:BTP-EH	0.860	23.8	76.2	15.2±0.29 (15.6)
D18:BTP-HD	0.898	22.3	68.6	13.1±0.31 (13.7)

Average values obtained from 10 independent devices for each active layer system. The best PCEs are provided in parentheses.

Table S7 Photovoltaic parameters of D18:BTP-C3 based *is*-OSCs under different strains.

Strain (%)	V_{OC} **(V)**	J_{SC} **(mA/cm^2)**	**FF (%)**	**PCE (%)**
0	0.853	23.1	75.4	14.4±0.33 (14.9)
10	0.843	23.0	73.5	13.9±0.33 (14.3)
20	0.851	22.3	66.5	12.3±0.29 (12.6)
30	0.843	21.1	61.2	10.2±0.32 (10.8)
40	0.844	16.8	39.2	5.1±0.39 (5.6)

Average values obtained from 10 independent devices for each active layer system. The best PCEs are provided in parentheses.

Table S8 Photovoltaic parameters of D18:BTP-EH based *is*-OSCs under different strains.

Strain (%)	V_{OC} **(V)**	J_{SC} **(mA/cm^2)**	**FF (%)**	**PCE (%)**
0	0.860	23.8	76.2	15.2±0.29 (15.6)
10	0.872	23.5	74.5	15.0±0.26 (15.3)
20	0.868	22.9	67.6	13.1±0.27 (13.4)
30	0.875	22.1	64.1	12.1±0.26 (12.4)
40	0.877	18.5	40.4	6.15±0.36 (6.6)

Average values obtained from 10 independent devices for each active layer system. The best PCEs are provided in parentheses.

Table S9 Photovoltaic parameters of D18:BTP-HD based *is*-OSCs under different strains.

Strain (%)	V_{OC} **(V)**	J_{SC} **(mA/cm^2)**	**FF (%)**	**PCE (%)**
0	0.898	22.3	68.6	13.1±0.31 (13.7)
10	0.895	22.1	68.2	13.0±0.32 (13.5)
20	0.894	21.7	65.5	12.1±0.34 (12.7)
30	0.897	20.4	63.0	11.2±0.28 (11.6)
40	0.876	16.4	51.6	6.9±0.33 (7.4)

Average values obtained from 10 independent devices for each active layer system. The best PCEs are provided in parentheses.

4. Supplementary References

1 J. Yuan, Y. Zhang, L. Zhou, G. Zhang, H.-L. Yip, T.-K. Lau, X. Lu, C. Zhu, H. Peng, P. A. Johnson, M. Leclerc, Y. Cao, J. Ulanski, Y. Li and Y. Zou, *Joule*, 2019, **3**, 1140-1151.

2 J. Han, F. Bao, D. Huang, X. Wang, C. Yang, R. Yang, X. Jian, J. Wang, X. Bao and J. Chu, *Adv. Funct. Mater.*, 2020, **30**, 2003654.

3 J.-W. Lee, B. S. Ma, H. J. Kim, T.-S. Kim and B. J. Kim, *JACS Au*, 2021, **1**, 612-622.

4 J.-W. Lee, D. Jeong, D. J. Kim, T. N.-L. Phan, J. S. Park, T.-S. Kim and B. J. Kim, *Energy Environ. Sci.*, 2021, **14**, 4067-4076.

5 Z. Peng, K. Jiang, Y. Qin, M. Li, N. Balar, B. T. O'Connor, H. Ade, L. Ye and Y. Geng, *Adv. Energy Mater.* , 2021, **11**, 2003506.

6 J. Huang, Z. Ren, Y. Zhang, K. Liu, H. Zhang, H. Tang, C. Yan, Z. Zheng and G. Li, *Adv. Funct. Mater.*, 2021, **31**, 2010172.

7 Z. Peng, K. Xian, Y. Cui, Q. Qi, J. Liu, Y. Xu, Y. Chai, C. Yang, J. Hou, Y. Geng and L. Ye, *Adv. Mater.* , 2021, **33**, 2106732.

8 Q. Wu, W. Wang, Y. Wu, Z. Chen, J. Guo, R. Sun, J. Guo, Y. Yang and J. Min, *Adv. Funct. Mater.*, 2021, **31**, 2010411.

9 R. Ma, K. Zhou, Y. Sun, T. Liu, Y. Kan, Y. Xiao, T. A. Dela Peña, Y. Li, X. Zou, Z. Xing, Z. Luo, K. S. Wong, X. Lu, L. Ye, H. Yan and K. Gao, *Matter*, 2022, **5**, 725-734.

10 J. Wang, Y. Cui, Y. Xu, K. Xian, P. Bi, Z. Chen, K. Zhou, L. Ma, T. Zhang, Y. Yang, Y. Zu, H. Yao, X. Hao, L. Ye and J. Hou, *Adv. Mater.*, 2022, **34**, 2205009.

11 J.-W. Lee, C. Sun, S.-W. Lee, G.-U. Kim, S. Li, C. Wang, T.-S. Kim, Y.-H. Kim and B. J. Kim, *Energy Environ. Sci.*, 2022, **15**, 4672-4685.

12 J. W. Lee, S. Seo, S. W. Lee, G. U. Kim, S. Han, T. N. L. Phan, S. Lee, S. Li, T. S. Kim, J. Y. Lee and B. J. Kim, *Adv. Mater.* , 2022, **34**, 2207544.

13 Q. Fan, R. Ma, W. Su, Q. Zhu, Z. Luo, K. Chen, Y. Tang, F. R. Lin, Y. Li, H. Yan, C. Yang, A. K. Y. Jen and W. Ma, *Carbon Ener.*, 2022, **5**, 267.

14 J. W. Lee, C. Lim, S. W. Lee, Y. Jeon, S. Lee, T. S. Kim, J. Y. Lee and B. J. Kim, *Adv. Energy Mater.* , 2022, **12**, 2202224.

15 W. Song, K. Yu, J. Ge, L. Xie, R. Zhou, R. Peng, X. Zhang, M. Yang, Z. Wei and Z. Ge, *Matter*, 2022, **5**, 1877-1889.

16 J. W. Lee, T. N. L. Phan, E. S. Oh, H. G. Lee, T. S. Kim and B. J. Kim, *Adv. Funct. Mater.*, 2023, **33**, 2301851.

17 J. Kim, G.-U. Kim, D. J. Kim, S. Lee, D. Jeong, S. Seo, S.-J. Ko, S. C. Yoon, T.-S. Kim and B. J. Kim, *J. Mater. Chem. A*, 2023, **11**, 4808-4817.

18 G. U. Kim, C. Choi, D. Jeong, D. J. Kim, T. N. L. Phan, S. Song, J. Park, T. S. Kim, Y. H. Kim and B. J. Kim, *Adv. Energy Mater.* , 2023, **13**, 2302125.

19 Q. Wan, S. Seo, S.-W. Lee, J. Lee, H. Jeon, T.-S. Kim, B. J. Kim and B. C. Thompson, *J. Am. Chem. Soc.*, 2023, **145**, 11914-11920.

20 S. Seo, J. W. Lee, D. J. Kim, D. Lee, T. N. L. Phan, J. Park, Z. Tan, S. Cho, T. S. Kim and B. J. Kim, *Adv. Mater.*, 2023, **35**, 2300230.

21 J. Huang, Z. Lu, J. He, H. Hu, Q. Liang, K. Liu, Z. Ren, Y. Zhang, H. Yu, Z. Zheng and G. Li, *Energy & Environmental Science*, 2023, **16**, 1251-1263.

22 M. Li, Z. Peng, K. Xian, W. Zhao, C. Liu, Y. Chen, C. Cui and L. Ye, *J. Mater. Chem. A*, 2023, **11**, 5606-5614.

23 M. Li, K. Xian, W. Zhao, D. Sheng, C. Liu, X. Li, W. Li and L. Ye, *Chem. Eng. J.*, 2023, **476**.
24 X. Zheng, X. Wu, Q. Wu, Y. Han, G. Ding, Y. Wang, Y. Kong, T. Chen, M. Wang, Y. Zhang, J. Xue, W. Fu, Q. Luo, C. Ma, W. Ma, L. Zuo, M. Shi and H. Chen, *Adv. Mater.*, 2023, **35**, 2307280.
25 J. Liu, W. Zhou, J. Deng, X. Geng, S. Y. Jeong, Y. Cui, H. Y. Woo, F. Wu, F. Liu and L. Chen, *Nano Energy*, 2024, **121**, 109218.
26 W. Tang, Z. Ding, Y. Su, Q. Weng, Y. Zhang, R. Li, W. Huang, Z. Wang, Y. Wu, Y. Han, K. Zhao, Z. Yang, X. Wang and S. Liu, *Adv. Funct. Mater.*, 2024, **34**, 2312289.
27 J.-W. Lee, H.-G. Lee, E. S. Oh, S.-W. Lee, T. N.-L. Phan, S. Li, T.-S. Kim and B. J. Kim, *Joule*, 2024, **8**, 204-223.
28 Q. Wan, H. Jeon, S. Seo, E. S. Oh, J.-W. Lee, C. Wang, T.-S. Kim, B. J. Kim and B. C. Thompson, *Chem. Mater.*, 2023, **35**, 10476-10486.
29 J. Zhang, Q. Chen, M. Li, G. Zhang, Z. Zhang, X. Deng, J. Xue, C. Zhao, C. Xiao, W. Ma and W. Li, *Adv. Mater.*, 2024, **36**, 2312805.
30 X. Li, H. Ke, S. Li, M. Gao, S. Li, J. Yu, H. Xie, K. Zhou, K. Zhang and L. Ye, *Adv. Funct. Mater.*, 2024, **34**, 2400702.